POAC'25
St. John's, Newfoundland and Labrador, Canada

Proceedings of the 28th International Conference on Port and Ocean Engineering under Arctic Conditions
Jul 13-17, 2025
St. John's, Newfoundland and Labrador
Canada

A Practical Method to Establish the Apparent Fracture Toughness of Ice in the Field

Sid S. Oksala[1], Pauli S. Lehto[1], Jukka A. Tuhkuri[1]
[1]Department of Energy and Mechanical Engineering, Aalto University, Espoo, Finland

ABSTRACT

There is a need to measure the apparent fracture toughness of ice in the field. Previously developed methods are laborious and consequently more practical methods would allow more data to be collected from a variety of settings, e.g. during short day trips and from onboard ships. To this end a compact and lightweight loading device was designed and constructed that could be used in the field. A digital control system was developed for the loading device that enables both load- and displacement-controlled tests. The device performs fracture tests with semi-circular bend specimens of 140 mm diameter, which can be easily cut from commonly collected ice cores. The design of the loading device is presented, and its compliance is compared to that of the specimens. The architecture of the digital control system is also presented, and the resolution of the measurement signals along with the different functions the system enables are explained. The system is then tested during a set of field experiments conducted at Van Mijenfjorden, Svalbard during March 2025. The accuracy of both the load- and displacement-control during these tests is discussed and the attained results are shown to be both comparable to and as repeatable as similar experiments conducted under laboratory conditions. Finally, the presented system is found to be a practical alternative to quickly measure the apparent fracture toughness of ice in the field.

KEY WORDS: Ice mechanics; Field work; Fracture mechanics; Sea ice; Experimental methods.

INTRODUCTION

Extensive experimental work has been conducted on the fracture mechanics of sea ice, remaining topical to date with significant effort being made to uncover the mechanisms and properties that govern the strength and fracture of sea ice. Whilst laboratory experiments can provide many useful insights, it is imperative to carry out field experiments as procuring ice that is representative of natural grown sea ice is challenging (Oksala et al. 2024). It is important that the methods employed during these field experiments are as practical as possible due to the challenging working conditions. Furthermore, if the methods employed are quick and efficient, field experiments can be conducted in a variety of different ways, e.g. from onboard ships with minimal stops, thus increasing the availability of data. Lastly, whatever methods are employed, they must provide consistent and reliable results. To this end an experimental method and loading device are developed in the current work, with the system employing a tailormade digital control system to ensure these requirements are met.

Previous methods to test the fracture properties of sea ice (namely the apparent fracture toughness, K_Q) have been typically done on large specimens by e.g. Dempsey et al. (1999) and Lu et al. (2015). The experiments proposed by Dempsey et al. (1999) involved cutting edge cracked rectangular plate specimens out of sea ice, having a varied specimen size with main dimensions ranging up to 80 m. The specimens were subsequently loaded using a flatjack until the fracture of the specimen. Dempsey et al. (1999) utilized the large specimen sizes to study the size effects in testing of sea ice, and to investigate how specimen size affects the apparent fracture toughness.

The size effects in sea ice have been recently investigated by Ahmad (2024) using digital image correlation to reveal the process zone ahead a crack tip. The results showed that the process zone size is of the order of millimetres, which indicates that it may be possible to carry out fracture toughness tests on a smaller scale than previously thought. Small ice samples are commonly extracted using ice cores, with the semi-circular bend (SCB) geometry often used both in and outside the ice mechanics field (e.g. Adamson et al. (1997) and LeClair et al. (1997), Kuruppu et al. (2014)). Typically experiments utilising the SCB geometry are done so that the cores are harvested on site and then transported to laboratories for testing at a later date for convenience. This transportation induces a level of uncertainty to the measurement results, since sea ice undergoes changes once it is removed from the sea (Weeks 2010). In this paper, we propose a detailed methodology that is suited to the field testing of SCB geometries at the location of ice core extraction. A digital control system and an electro-mechanical loading device are developed to ensure accurate control and precise data acquisition. Consequently, the tests are carried out using a closed-loop control algorithm that enables exact loading sequences to be determined, contrary to the previous field experiments. This also makes it possible to carry out both load and displacement-controlled tests.

LOADING DEVICE

The loading device has an aluminium profile base (100 mm by 200 mm Bosh Rexroth) to support the ice sample and displacement sensors, two 10 mm thick stainless-steel A-frames, and an aluminium profile cross piece (45 mm by 90 mm Bosh Rexroth) at the top. A linear actuator is attached to this cross piece by a 10 mm stainless steel gantry plate. The linear

actuator moves using a ball screw and two sliding blocks. It has a stroke of 70 mm and a dynamic load rating of 1.83 kN. On top of the linear actuator is a stepper motor (rated torque of 1.85 Nm) and a 1:50 reduction gearbox. On the bottom of the linear actuator is a load cell and loading tip. A CAD model of the loading device can be seen in Figure 1 (left).

The crack mouth opening displacement (CMOD) is measured using two laser triangulation displacement sensors. The laser sensors reference aluminium L-profiles that are screwed and/or frozen to the edges of the crack mouth as shown in Figure 1. The summed signal from the two sensors is used as the control signal for displacement-controlled tests.

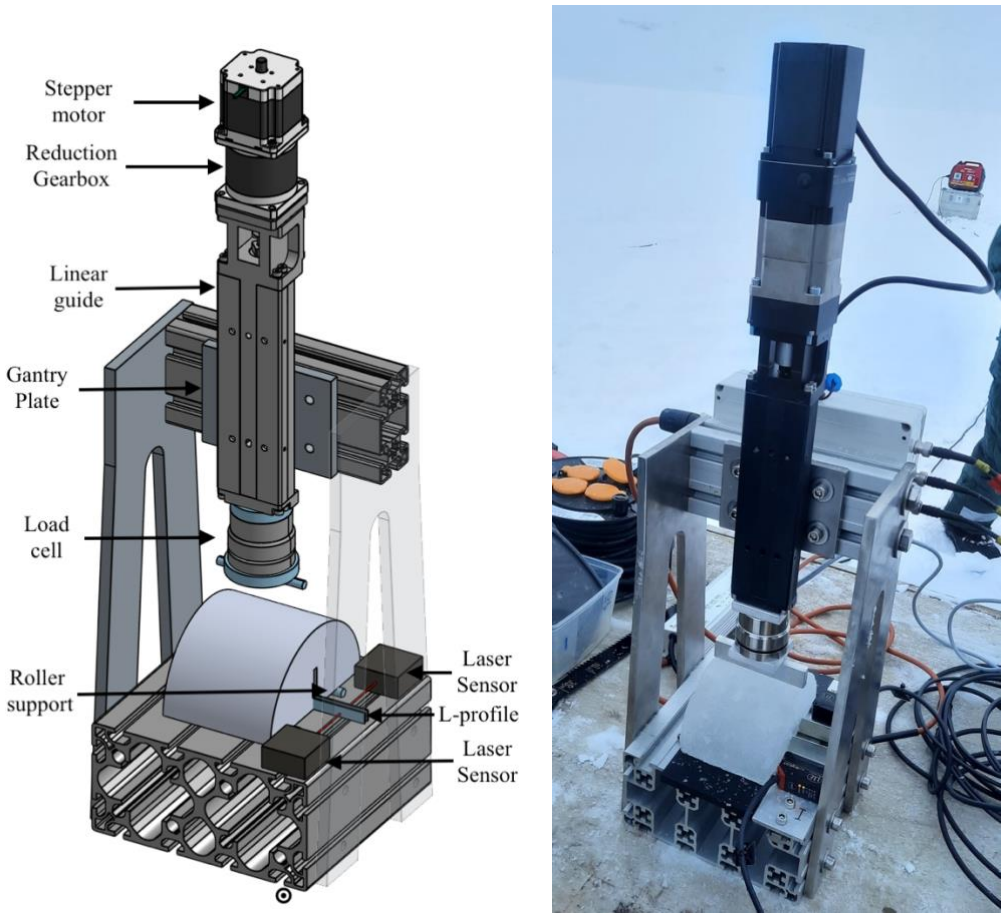

Figure 1. (left) Loading device CAD model (right) loading device in use in the Van Mijenfjorden, Svalbard in March 2025.

To be able to study the properties of a material, one must be sure that the response of the loading device itself is insignificant when compared to that of the material. Consequently, this design was made to be as stiff as possible. The stiffness of the loading device was tested in laboratory conditions. Both the horizontal and vertical displacement of the gantry plate was measured relative to the base whilst applying a steadily increasing load. At 90% of the rated load (1.65 kN) the loading was released and the recovery observed. The results of this test can be seen in Figure 2. At the maximum applied load of 1.65 kN the vertical displacement of the gantry plate reaches its maximum of 49.4 μm. Once the load is released the vertical displacement is recovered to within 1.5 μm of the preloading position. From Figure 2 a., it can also be seen that the horizontal displacement of the gantry plate is much smaller in magnitude, albeit it does not

return exactly to the initial value once the load is removed. However, the CMOD measurement is not affected by lateral movement, and the sample can move on its roller supports. Therefore, the horizontal displacement is unlikely to cause a release of elastic energy during a fracture event and this horizontal movement is not of concern. The vertical stiffness of the loading device is 32.2 kN/mm, as shown in Figure 2b. This value can be compared to field experiments conducted by Adamson et al. (1997) where the vertical stiffness of the ice samples can be calculated to be approximately 1.75 – 2.5 kN / 16-19 mm, which converts to average vertical stiffness of approximately 0.124 kN/mm. Thus, the stiffness of the developed loading device is estimated to be approximately 250 times stiffer than the ice samples, and thus the compliance of the loading device is sufficiently small.

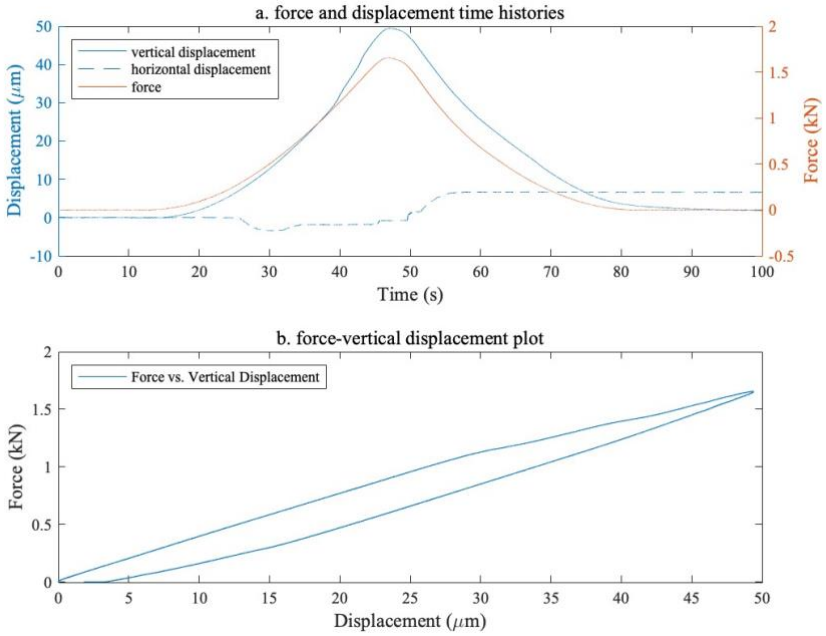

Figure 2. a. Gantry plate displacement and loading force as a function of time, b. Loading force plotted as a function of vertical displacement.

CONTROL AND DAQ SYSTEM

The digital control system has been developed at the Aalto University Solid Mechanics Laboratory. The software has been developed using National Instruments (NI) LabVIEW 2021. The hardware architecture has been developed in-house using the modular NI compactRIO 9054 controller, equipped with a real-time (RT) CPU and a Field Programmable Gate Array (FPGA). Interfacing with the test system's sensors and control elements is carried out through analogue and digital input and output (I/O) using the following NI C-series modules: NI9220, NI9269, NI9421, NI9474. The CMOD is measured using ILD 1420-10 laser displacement sensors manufactured by Micro-Epsilon. They have a 10 mm range, and a 4-20 mA output with a 16-bit resolution. The load cell used is a HBM U3 loadcell with a 10 kN range. The following signal conditioners are used for the instrumentation: 1) LEG GmbH TV5N current to voltage converters (4-20 mA to ±10V) for laser displacement sensors, and 2) LEG GmbH DM2 strain gage amplifiers for the load cell. The strain gage amplifiers were calibrated with a digital HBM

QuantumX MX410B universal amplifier as a reference. For the full compressive force range, the maximum deviation between the digital control system and the reference amplifier was ≤0.05%. Typical noise levels in force and displacement signals are 2N and 0.6 µm respectively.

The hardware and software architecture are depicted in Figure 3. For accurate control of the test system and to guarantee timing accuracy and eliminate jitter, a PID-control algorithm is implemented on the FPGA. The control algorithm has two control modes, 1) displacement control mode, and 2) force control mode, allowing seamless transition between the control modes.

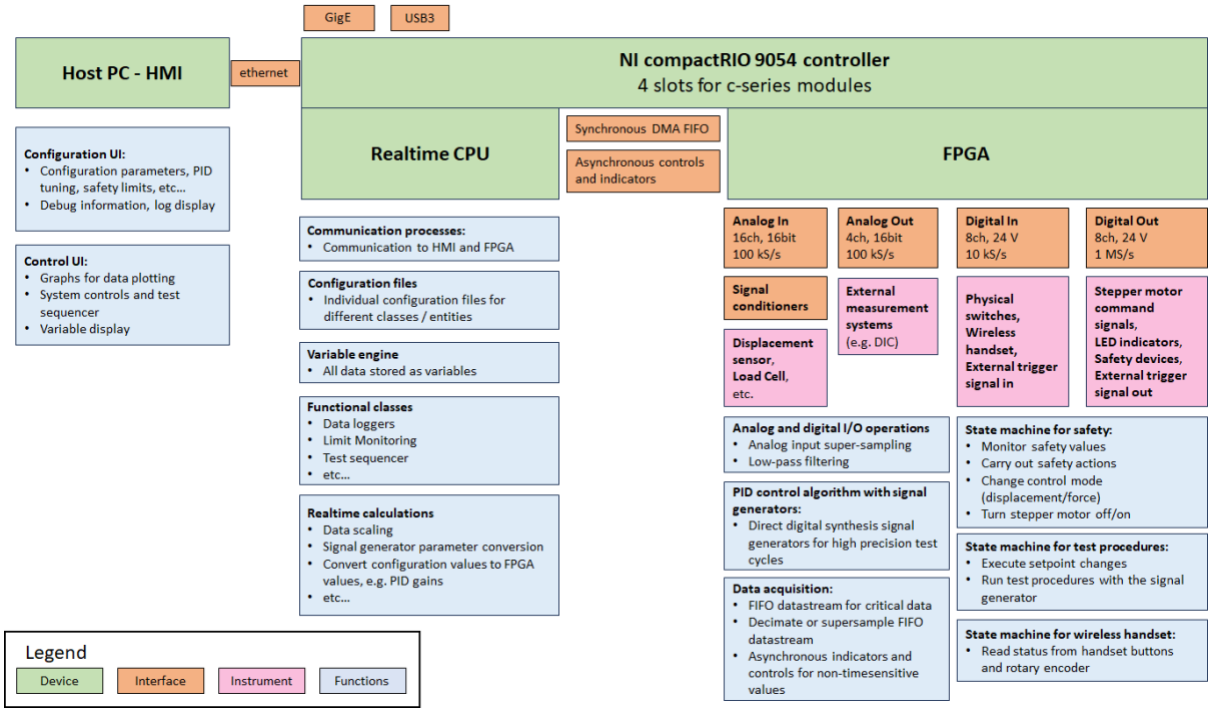

Figure 3. Hardware and software architecture for the digital control system.

All time-critical actions, including analogue and digital I/O interfaces, are also implemented onto the FPGA code. In parallel to the PID-control loop, individual state machines carry out safety limit monitoring and actions, run test procedures, and converts actions done with the wireless handset into commands for the stepper motor. The FPGA runs with a base clock of 40 MHz, and 16 channels of analogue input is sampled at 100 kHz at a resolution of 16 bits. A super-sampling factor of 20 is used, resulting in an effective control and sample rate of 5 kHz. Super sampling reduces signal noise and improves analogue input's effective resolution to approximately 18.2 bits. The stepper motor is driven with a combination of a digital pulse signal and a direction signal. The pulses are generated in a 40 MHz timed loop, with a timing precision of 25 ns.

The data from the FPGA is relayed synchronously through a DMA FIFO interface (Direct memory access, First-In-First-Out) to the RT CPU for further actions. The RT CPU transfers data through ethernet to the Host PC, which has the Human-Machine-Interface (HMI). The compactRIO operates independently of the Host PC, and upon a loss of connection safety actions are carried out (4 second grace period). The HMI is split into two user interfaces (UI): Configuration UI and Control UI. Using the Configuration UI, the user may e.g. change the

base configuration parameters of the system, set safety limits, change the PID gains, and adjust parameters for the data loggers.

With the Control UI, the variable data is shown with numeric indicators and graphical plots. Commands from the UI to the loading device are sent using manual setpoint changes or through the test sequencer. The sequencer has a *manual mode* to run the signal generator with fixed parameters, as well as an *automatic mode* which runs test sequences with text-based script files. Using the *automatic mode*, it is possible to flexibly tailor test procedures to include event detection, while and if loops, and dynamic adjustment of test parameters.

Most test procedures are dependent on the FPGA's signal generator, which is implemented using direct digital synthesis (DDS). In addition to the basic waveforms (linear, sinusoidal, triangle), custom waveforms can be sent from the HMI. This makes it possible to have very diverse test cycles, and to e.g. superimpose multiple waveforms (linear + sinusoidal) or use completely arbitrary waveforms. The loading device can also be controlled via a wireless handset, which can be used either in *closed-loop mode* to adjust the PID setpoint, or in *open-loop mode* to give direct speed commands to the stepper motor. The latter is used in the beginning of the test sequence to establish contact between the specimen and the loading device. For a more detailed description of the control system, refer to Aalto University Wiki (Lehto 2025).

SPECIMEN PREPARATION

The specimen preparation procedure is based on that described by Kuruppu et al. (2014) with some modifications to make the procedure more applicable to ice. The samples are harvested using a Kovacs Mark V ice coring system. The ice core (D = 140 mm) is then sliced into sections along the coring direction (h = 100 mm), which are then cut in half producing the semicircular bend specimens. A blade as thin as possible should be used for this. It is vital that the cut through the diameter is straight, and that the cutting width is as narrow as possible. Here an electric chainsaw was found to produce a sufficiently flat and straight surface for mounting the sample in the loading device. To complete the test specimen geometry, a notch is cut into the middle of the sample. Kuruppu et al. (2014) report that this notch should be between 0.4 and 0.6 times the radius (a = 0.4R…0.6R). Our preliminary trials with the device have shown that for saline ice 0.5R is sufficient but that for freshwater ice a notch as long 0.7R may be necessary to attain both sufficient compliance of the sample and adequate CMOD response to loading. The sample along with the indicated dimensions is shown in Figure 4, and Table 1 summarizes the justifications for the chosen dimensions.

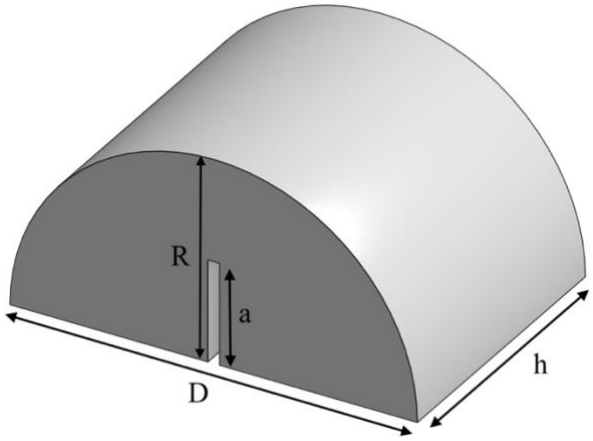

Figure 4. Illustration of prepared sample

Table 1. Dimensions of sample

Dimension	Value	Explanation
Diameter (D)	140 mm	Kuruppu et al. (2014) report D > 10 times grain size, 140 mm chosen based on Kovacs availabilities
Radius (R)	70 mm	Should be measured for each specimen, 65 - 70 mm depending on saw used to cut specimen
Thickness (h)	100 mm	Kuruppu et al. (2014) report 0.4D, however 100 mm was chosen based on Ahmad (2024)
Notch (a)	35 mm	Kuruppu et al. (2014) report 0.4R – 0.6R. Based on trials 0.5R was suitable for saline ice, and 0.7R for freshwater ice

Once the sample has been prepared aluminium plates are attached to both sides of the crack face to act as targets for the laser displacement sensors. Depending on the conditions these can be attached either by simply freezing them to the sample or by using small screws (e.g. 3.5X6.5). The sample is then placed in the loading device on two stainless steel rollers of 6 mm diameter placed 105 mm apart, centre to centre and the laser displacement transducers are positioned approximately in the centre of their measurement range. Thereafter, the operator uses the HMI to enable and control the stepper motor in open loop control using the wireless handset and starts the test sequencer. The sequencer starts data-logging and waits until a pre-determined contact force level is reached, after which the system automatically switches to the closed-loop PID control and performs a linear loading ramp until the failure of the specimen. Tests can be carried out both under displacement and force control. Typical loading rates for load- and displacement-controlled experiments range from 10 N/s to 100 N/s and 1 μm/s to 10 μm/s respectively.

FIELD TRIALS

The loading device was field tested on sea ice in the Van Mijenfjorden, Svalbard between the 26th and the 28th of March 2025. In total 22 experiments were conducted. Of these experiments, 6 were conducted to test the functionality of the loading device. Of these experiments 5 were

displacement controlled and 1 was load controlled. During the field work ambient air temperatures ranged between −9 °C and −5 °C. The average ice thickness was 63 cm with an average of 30 cm of snow on top. The salinity of the ice ranged between 4 ppt and 9 ppt. A summary of the experiments conducted to test the capabilities of the loading device can be seen in Table 2, showing the control mode type, dimensions of the specimen, maximum load, apparent fracture toughness, location of the sample from the top of the ice core and the sample temperature at the end of the test. Detailed analysis of mechanical response of the ice specimens are beyond the scope of the current work and will be published separately.

Table 2. Summary of experiments conducted to test the capabilities of the loading device.

Core #	Experiment Type	Dimensions (mm)	Load (N)	K_Q (kPa√m)	Depth (cm)	Ice temperature (°C)
1	Disp. control	R = 71, a = 38, h = 98	277	44.7	0	- 6.8
1	Disp. control	R = 65, a = 40, h = 98	186	44.4	0	- 6.8
2	Load control	R = 66, a = 40, h = 97	253	58.9	0	- 4.6
2	Disp. control	R = 72, a = 46, h = 98	304	67.6	10	- 4.2
2	Disp. control	R = 67, a = 45, h = 96	256	72.7	20	- 5.5
2	Disp. control	R = 71, a = 40, h = 94	353	65.2	30	- 4.7

The apparent fracture toughness values have been calculated using equations (1) and (2) (Kuruppu et al., 2014).

$$K_Q = Y' \frac{P_{max}\sqrt{\pi a}}{2Rh} \tag{1}$$

where,

$$Y' = -1.297 + 4.758\frac{s}{R} - \left(0.47 + 8.229\frac{s}{R}\right)\frac{a}{R} + \left(1.071 + 17.201\frac{s}{R}\right)\left(\frac{a}{R}\right)^2 \tag{2}$$

with s being the span length of the bottom roller supports, and P_{max} being the load at fracture.

Typical time history plots of displacement and load control experiment can be seen in Figure 5 a. and 5 b. The short non-linear regions in the beginning corresponds to the loading device being driven to contact manually by the operator, and an initial build-up of compressive load. The following linear region that lasts the majority of the tests represents the automated portion where the PID control is in effect. The final section where the deviation from the target grows substantially corresponds to the failure of the specimen.

Figures 5 c. and 5 d. present typical deviations between the target value of the linear ramp and measured displacement or load signals. In the case of the displacement-controlled tests the deviation is typically less than ±1 µm. For the load-controlled tests the deviation remains within the noise band of load cell (approximately ±2 N), with a slight averaged increase towards the end of the test. Since the magnitude of both these deviations is of the same order as the lowest loading rate, they can be considered acceptable especially considering the measurement range of the displacement sensor and load cell.

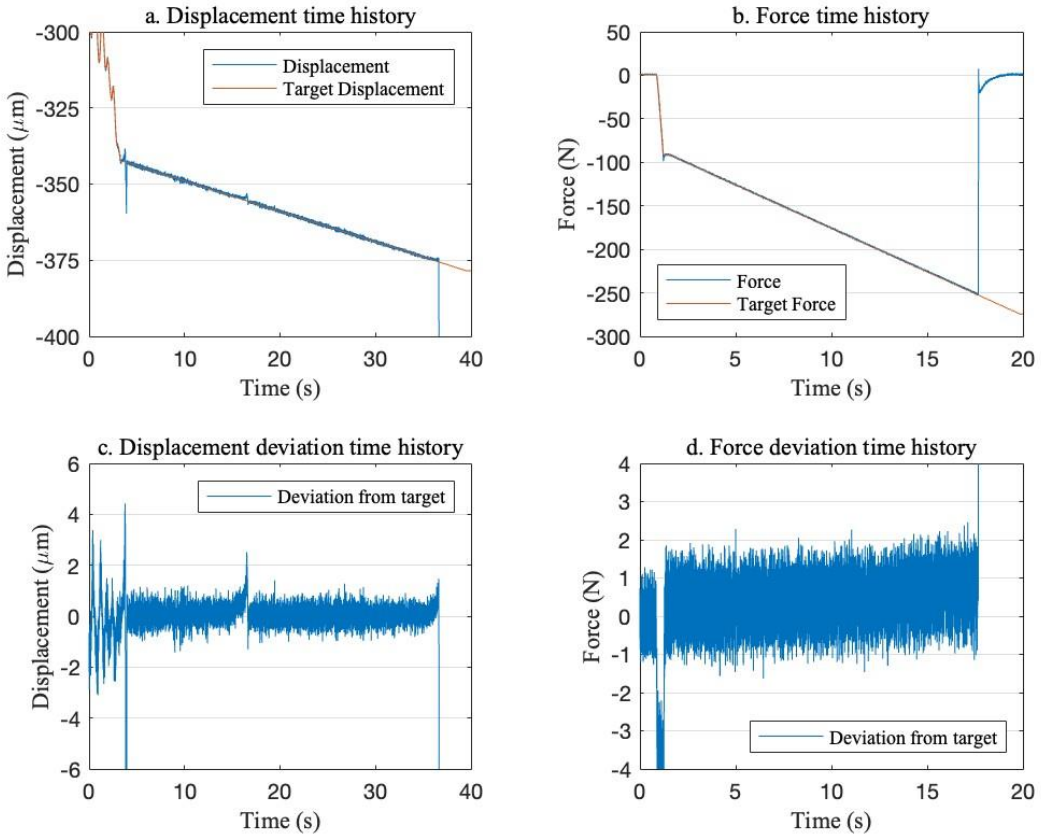

Figure 5. a. Time history of both measured displacement and target displacement during typical displacement-controlled experiment, b. Time history of both measured load and target load during typical load-controlled experiment, c. Deviation of measured displacement from target displacement during displacement-controlled experiment, and d. Deviation of measured load from target load during load-controlled experiment.

DISCUSSION

There is a need to measure the apparent fracture toughness of ice in the field practically and quickly. To this end a loading device and digital control system was created. The system was field tested in the Van Mijenfjorden, Svalbard in March of 2025. Six experiments were conducted to test the capabilities of the developed system. Of these experiments 5 were displacement controlled and 1 was load controlled. The aim was to see whether the values attained with the developed system were comparable to those reported by others.

Typically reported values for the apparent fracture toughness of ice range from 20 kPa√m to over 200 kPa√m depending on the type of ice and the type of tests among other things (e.g. Adamson et al. (1997) and El Gharamti (2021)). Adamson et al. (1997) report apparent fracture toughness values for similar sized SCB specimens of naturally grown sea ice tested both in a laboratory at -12 °C and in the field at -38 °C. They found the mean apparent fracture toughness to be 49.5 kPa√m with a standard deviation of 11.4 and 120.7 kPa√m with a standard deviation of 13.1 for the laboratory and field experiments respectively. The experiments were done with

consideration to the c-axis alignment of the ice. The results attained while testing and tuning the PID control of the device presented in this paper had a mean of 58.9 kPa√m and a standard deviation of 12.0 with no regard to c-axis orientation. Since there is a good agreement between the mean values attained here to experiments conducted under similar temperatures in a laboratory, and the presented device is able to reach standard deviation values close to those attained under laboratory conditions, the presented method can be considered a good alternative to the laboratory experiments conducted by Adamson et al. (1997).

LeClair et al. (1997) reported similar experiments conducted in a cold room at -10 °C, with significantly higher values for apparent fracture toughness. From their data a mean value of 90.4 kPa√m with a standard deviation of 11.9 can be calculated for samples tested perpendicular to the c-axis and 95.2 kPa√m with a standard deviation of 9.4 can be calculated for samples tested parallel to the c-axis. The significantly higher values attained by LeClair et al. (1997) under similar temperature conditions can potentially be explained by the effects of temperature cycling on the ice during storage (eg. Weeks 2010). However, what should be noted here, is that they attain roughly a similar amount of scatter under laboratory conditions as the presented method does under field conditions, further reinforcing the suitability of the presented method as an alternative to laboratory experiments.

SUMMARY AND CONCLUSIONS

A portable loading device and associated control system was developed to test the apparent fracture toughness of ice in the field. The stiffness of the device was tested in the laboratory before it underwent field trials and was found to be sufficient for the intended purpose. During these field trials conducted in Svalbard during March 2025 both load- and displacement-controlled tests were conducted. The accuracy of the used control system during these tests was found to be excellent. Based on these tests the apparent fracture toughness was calculated and compared to literature values. A good agreement between the two was found. The presented 140 mm diameter core-based method that utilises precise digital control to test the apparent fracture toughness of ice in the field is shown to be a practical alternative to previously developed methods without closed-loop control for fracture tests in the field.

ACKNOWLEDGEMENTS

We would like to thank the Research Council of Finland for funding the project. Sid Oksala would like to thank Mohammad Izadi, Veijo Laukkanen, Otto Puolakka, Lasse Turja, and Teemu Päivärinta for their help in designing and building the loading device. Sid Oksala would also like to thank Knut Hoyland, Marine Ilg, and UNIS for arranging the field work, The Research Council of Norway for funding his part of the field work, and Aleksey Marchenko, Martin Ludvigsen, Tim Hammer, Alexandra Pliss, Marius Stübbe and the students of the course AT-311/811 for their help during the field work.

REFERENCES

Adamson, R.M., Shapiro, L.H. and Dempsey, J.P., 1997. Core-based SCB fracture of aligned first-year sea ice (phases III and IV). Journal of cold regions engineering, 11(1), pp.30-44.

Ahmad, W., 2024. Understanding ice fracture using Digital Image Correlation-From microstructural crack arrest to comparison with the visco-elastic fictitious crack model.

Dempsey, J.P., Adamson, R.M. and Mulmule, S.V., 1999. Scale effects on the in-situ tensile strength and fracture of ice. Part II: First-year sea ice at Resolute, NWT. International journal of fracture, 95(1), pp.347-366.

Gharamti, I.E., Dempsey, J.P., Polojärvi, A. and Tuhkuri, J., 2021. Fracture of warm S2 columnar freshwater ice: size and rate effects. Acta Materialia, 202, pp.22-34.

Kuruppu, M.D., Obara, Y., Ayatollahi, M.R., Chong, K.P. and Funatsu, T., 2014. ISRM-suggested method for determining the mode I static fracture toughness using semi-circular bend specimen. Rock Mechanics and Rock Engineering, 47, pp.267-274.

LeClair, E.S., Adamson, R.M. and Dempsey, J.P., 1997. Core-based SCB fracture of aligned first-year sea ice (Phase VI). Journal of cold regions engineering, 11(1), pp.45-58.

Lehto, P, 2025. Aalto University Wiki: Aalto University Solid Mechanics Laboratory. Available at: https://wiki.aalto.fi/display/SMLab, Accessed: 2/4/2025.

Lu, W., Løset, S., Shestov, A. and Lubbad, R., 2015. Design of a field test for measuring the fracture toughness of sea ice. In Proceedings of the International Conference on Port and Ocean Engineering Under Arctic Conditions.

Oksala, S., Puolakka, O., Izadi, M. and Tuhkuri, J., 2024. Salinity-controlled laboratory production of ice. In International Association for Hydro-Environment Engineering and Research International Symposium on Ice. International Association for Hydro-Environment Engineering and Research.

Schulson, E.M. and Duval, P., 2009. Creep and fracture of ice. Cambridge university press.

Urabe, N., Iwasaki, T. and Yoshitake, A., 1980. Fracture toughness of sea ice. Cold Regions Science and Technology, 3(1), pp.29-37.

Weeks, W., 2010. On sea ice. University of Alaska Press.